© 2019. Published by The Company of Biologists Ltd | Development (2019) 146, dev171397. doi:10.1242/dev.171397

RESEARCH REPORT

Transient localization of the Arp2/3 complex initiates neuronal dendrite branching *in vivo*

Tomke Stürner[1,§], Anastasia Tatarnikova[1,2,§,¶], Jan Mueller[3,*], Barbara Schaffran[1], Hermann Cuntz[4,5], Yun Zhang[1,‡], Maria Nemethova[3,*], Sven Bogdan[6], Vic Small[3] and Gaia Tavosanis[1,]**

ABSTRACT

The formation of neuronal dendrite branches is fundamental for the wiring and function of the nervous system. Indeed, dendrite branching enhances the coverage of the neuron's receptive field and modulates the initial processing of incoming stimuli. Complex dendrite patterns are achieved *in vivo* through a dynamic process of *de novo* branch formation, branch extension and retraction. The first step towards branch formation is the generation of a dynamic filopodium-like branchlet. The mechanisms underlying the initiation of dendrite branchlets are therefore crucial to the shaping of dendrites. Through *in vivo* time-lapse imaging of the subcellular localization of actin during the process of branching of *Drosophila* larva sensory neurons, combined with genetic analysis and electron tomography, we have identified the Actin-related protein (Arp) 2/3 complex as the major actin nucleator involved in the initiation of dendrite branchlet formation, under the control of the activator WAVE and of the small GTPase Rac1. Transient recruitment of an Arp2/3 component marks the site of branchlet initiation *in vivo*. These data position the activation of Arp2/3 as an early hub for the initiation of branchlet formation.

KEY WORDS: Neuron, Dendrite, Actin, Arp2/3, WAVE, Time-lapse imaging

INTRODUCTION

Neurons extend branched dendrites to establish appropriate connections within a circuit. Dendrite branching enhances the coverage of the receptive field of a neuron and modulates the initial processing of incoming stimuli. Complex dendrite patterns are achieved *in vivo* through a dynamic process of branch extension and retraction that initiates with the formation of a filopodium-like dendrite branchlet (Jontes et al., 2000; Kaethner and Stuermer, 1997; Sugimura et al., 2003; Wu et al., 1999). Branchlets are generally short processes of less than 30 µm in length, but their appearance and distinct dynamics vary among different types of neuron (Nagel et al., 2012). Only a subset of these dynamic branchlets is stabilized and can elongate into bona fide branches that remain for extended periods of time with the potential of branching further, while most disappear within a range of minutes to hours (Dailey and Smith, 1996; Heiman and Shaham, 2010; Niell et al., 2004). The initial step that allows the initiation of a dendrite branchlet is thus key to elaborating dendrite morphologies.

Actin is expected to play a central role in the formation of dynamic dendrite branchlets. Super-resolution microscopy recently revealed details of the organization of the actin cytoskeleton in dendrites, including periodical actin rings (D'Este et al., 2015). Additionally, patches of actin were observed in dendrites in electron microscopy preparations of primary hippocampal neuron cultures, as well as in pyramidal cells of the adult mouse cortex imaged *in vivo* with stimulated emission depletion (STED) nanoscopy (Korobova and Svitkina, 2010; Willig et al., 2014). These actin patches contain the actin nucleator complex Actin-Related Protein 2/3 (Arp2/3) and give rise to dendrite spines (Korobova and Svitkina, 2010; Saarikangas et al., 2015). However, the dynamic structure of actin supporting the process of bona fide dendrite branch formation has not been clarified. In *Drosophila* sensory class III dendritic arborisation (cIIIda) neurons, the formation of dendrite branchlets is predicted by the accumulation of a marker for dynamic F-actin: GMA (Andersen et al., 2005). GMA is a genetically encoded GFP-tagged actin-binding domain of moesin (Edwards et al., 1997) and its accumulation suggests a rapid remodelling or nucleation of actin at the site of branch formation. Additionally, GMA and LifeAct, an alternative F-actin marker, localize in dynamic puncta in *Drosophila* sensory class IV da (cIVda) neurons, at sites of new branch formation (Nithianandam and Chien, 2018). The Arp2/3 complex is a strong candidate for reshaping actin at the site of branch formation, as it promotes dendrite branching in cultured hippocampal neurons (Dharmalingam et al., 2009; Zhang et al., 2017) and is a major target of the small GTPase Rac1, a conserved key regulator of dendrite morphology (Govek et al., 2005).

Combining *in vivo* time-lapse analysis of fluorescently tagged actin regulators in da neurons, genetic analysis and electron tomography, we demonstrate that the Arp2/3 complex is the major actin nucleator involved in the initiation of dendrite branchlet formation, under the control of the suppressor of cAMP receptor/WASP family verprolin homology protein (SCAR/WAVE). Our data reveal a fundamental mechanism for dendrite branch formation via actin remodelling.

RESULTS AND DISCUSSION

To address the specific regulatory events at the core of the process of initial dendrite branch formation, we concentrated on the *Drosophila* larval sensory da neurons (Gao et al., 1999; Jan and Jan, 2010; Singhania and Grueber, 2014). These fall into four morphologically and functionally distinct neuronal subclasses, which range from the

[1]Deutsches Zentrum für Neurodegenerative Erkrankungen e.V./German Center for Neurodegenerative Diseases (DZNE), 53127 Bonn, Germany. [2]MPI for Neurobiology, 82152 Munich- Martinsried, Germany. [3]Institute of Molecular biotechnology (IMBA), 1030 Wien, Austria. [4]Ernst Strüngmann Institute (ESI) for Neuroscience in Cooperation with Max Planck Society, 60528 Frankfurt, Germany. [5]Frankfurt Institute for Advanced Studies, 60438 Frankfurt, Germany. [6]Institut für Physiologie und Pathophysiologie, Abteilung Molekulare Zellphysiologie, Phillips-Universität Marburg, 35037 Marburg, Germany.
*Present address: IST Austria, 3400 Klosterneuburg, Austria. ‡Present Address: School of Life Science, Sun Yat-Sen University, 510275 Guangzhou, PR China. §These authors contributed equally to this work ¶Deceased

**Author for correspondence (gaia.tavosanis@dzne.de)

G.T., 0000-0002-8679-5515

Received 7 September 2018; Accepted 8 March 2019

Development (2019) 146, dev171397. doi:10.1242/dev.171397

simple cIda to the complex cIIIda and space-filling cIVda neurons (Grueber et al., 2002). We first investigated the dynamics of actin enrichment within differentiating cIVda neuron dendrites in live second instar larvae. Dynamic actin, highlighted by GMA (Edwards et al., 1997), was enriched within the distal dendrite branches, which exhibit a higher rate of *de novo* branchlet formation (Fig. 1A). It displayed a highly dynamic localization with GMA puncta, as well as longer stretches of GMA enrichment forming and disappearing within minutes (Fig. 1C,D; Movie 1). Although transient GMA enrichment did not per se predict a site of *de novo* branch formation, the appearance of a novel branchlet was preceded by a persistent punctum of GMA enrichment. Indeed, 90% of all analysed *de novo* branch formation events showed actin accumulation of more than 30% relative to the basal level (n=85) (Fig. 1B). These data indicate that polymerization of actin is highly dynamic during dendrite differentiation in cIVda neurons. Moreover, they suggest that actin polymerization is a required step but does not suffice for the formation of a novel branch.

The initial assembly of an actin filament requires actin nucleators that stabilize the first seed of G-actin molecules (Firat-Karalar and Welch, 2011; Rottner et al., 2017). Therefore, to reveal the molecular machinery underlying branch formation, we performed a late cell-autonomous knockdown in cIda, cIIIda and cIVda neurons of actin nucleators, including the formins Capu, dDAAM, Dia, Fhos, FMNL and Formin3, the WH2 domain protein Spire, and components of the Arp2/3 complex (Dietzl et al., 2007). This approach allowed bypassing the initial phase of neuronal polarity establishment and primary neurite elongation to observe specific effects during terminal dendritic branching. The knock down of subunits of the Arp2/3 complex, including Arp2, Arp3 or Arpc1, strongly reduced the number of dendrite branches in cIVda (Fig. S1A,D) and cIIIda neurons (Fig. S1B,E). Although the primary branches (Fig. S1D-F) were not modified, other branch orders were reduced in number in cIVda and cIIIda neurons (Fig. S1D,E).

We thus addressed the *in vivo* role of Arp2/3 in dendrite branchlet formation. Using mosaic analysis with a repressible cell marker (MARCM) (Lee and Luo, 1999), we generated single cIVda neuron clones carrying null mutations of the Arp2/3 subunit *Arpc1* (*Arpc1*^{Q25sd} or *Arpc1*^{R337st}) (Hudson and Cooley, 2002; Zallen et al., 2002). These two alleles led to a strong reduction in overall branch density in cIVda neurons, validating the RNAi phenotype (Fig. 2A-C,E). In addition, in *Arpc1*^{Q25sd} mutant clones, high order

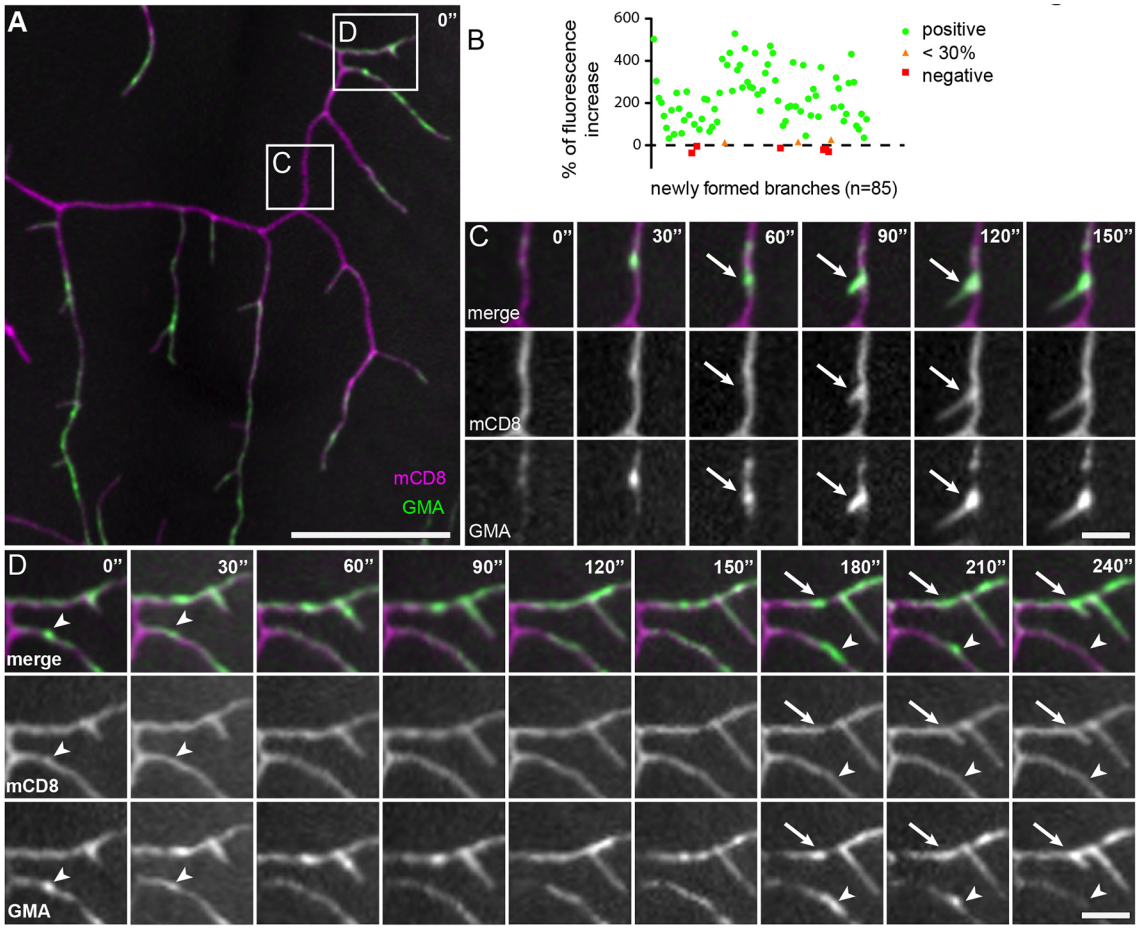

Fig. 1. Actin localization is highly dynamic in dendrite branches of differentiating cIVda neurons. (A) Localization of dynamic actin (GMA, green) within dendrite branches of differentiating cIVda neurons of second instar larvae. Dendrites dynamics are visualized using mCD8-cherry (magenta; genotype *Gal4*$^{109(2)80}$*/ +; UAS-mCD8-Cherry/UAS-GMA*). The initial image of a time-lapse series is shown here (see Movie 1). Scale bar: 50 µm. (B) Distribution of the percentage of increase in signal above background at the site of new branch formation for 85 recorded events. Green dots indicate events in which more than 30% increase in signal above background was recorded 30 s before branch initiation (89.4% of events). In three instances, the increase was lower than 30% (3.5% of events, orange triangles) and in six instances there was no increase (7% of events, red squares). (C,D) Magnification of the two boxed regions in A. 2.5 min (C) and 4 min (D) of this time-lapse series are shown, with arrows indicating the sites of new branch formation. Arrowheads in D indicate a site of actin accumulation that is not followed by the formation of a branch within the imaging time. Scale bar: 10 µm. n=10 movies.

Development (2019) 146, dev171397. doi:10.1242/dev.171397

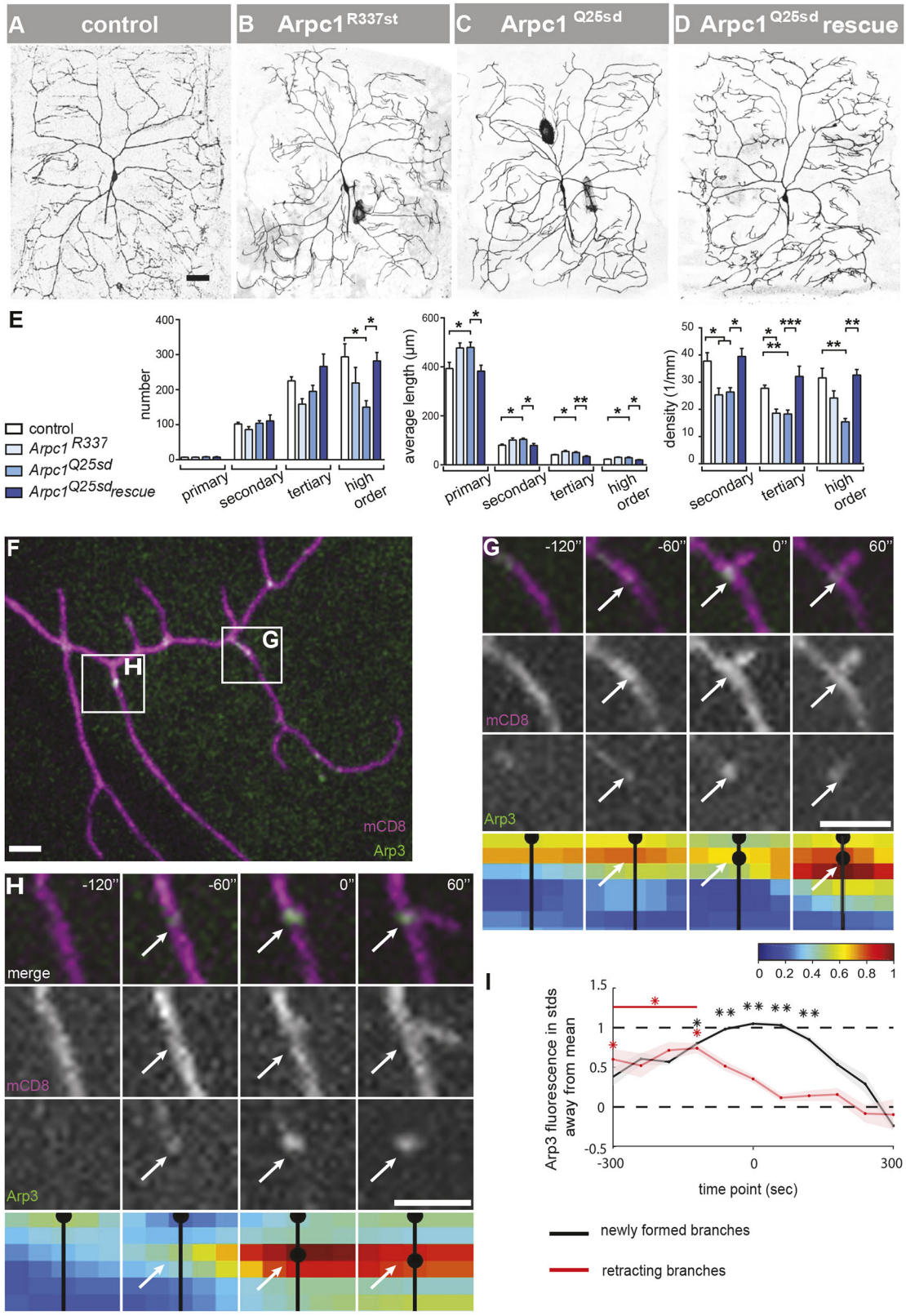

Fig. 2. See next page for legend.

branch number was reduced and average branch length increased (Fig. 2E). The cIVda neuron phenotype was rescued by expressing *Arpc1-GFP* in the mutant neurons (Hudson and Cooley, 2002), demonstrating that the dendrite branching phenotype derives from the loss of Arpc1 function and that Arpc1 is required cell-autonomously (Fig. 2D,E).

To distinguish whether the reduction in the number of branches observed upon loss of Arp2/3 function is due to a defect in branch

Development (2019) 146, dev171397. doi:10.1242/dev.171397

Fig. 2. The Arp2/3 complex supports cIVda dendrite branching and transiently localizes at branching points. (A-D) A single ddaC neuron clone obtained by MARCM of control neurons (A), of neurons mutant for *Arpc1* (*Arpc1*^{R337st} allele) (B) or for *Arpc1*^{Q25sd} (C) alleles, or of neurons mutant for *Arpc1*^{Q25sd} but expressing GFP-tagged full-length Arpc1 (D). Scale bar: 50 µm. *n*=5. (E) Average number of dendrite branches, average length of dendrite branches and branch density in the analysed genotypes [*P≤0.05; **P≤0.01; ***P≤0.001]. (F) Time-lapse imaging of differentiating class IV ddaC neurons of second instar larvae expressing Arp3-GFP (green) and mCD8cherry (magenta) imaged every 60 s. (G,H) Three-minute time lapse of the regions boxed in F. Arrows indicate the sites where new branchlets will form. The panel series below represents, using a heat map, the enrichment of Arp3-GFP observed in the time-lapse at the various time points (dots are branching sites; see supplementary Materials and Methods). Scale bars: 10 µm. *n*=18. (I) Summary of Arp3-GFP fluorescence at appearing (black line) and disappearing (red line) branch points relative to the standard deviation of fluorescence on the remaining part of the branch (74 dendritic paths analysed). The straight lines indicate the mean fluorescence; shaded areas indicate the standard deviations around the mean.

formation or to an increased rate of branch retraction, we studied dendrite branching dynamics using time-lapse imaging of class IV ddaC neurons of second instar larvae expressing control or *Arp2* RNAi constructs. ddaC neurons in which *Arp2* was knocked down had a much lower rate of *de novo* dendrite branch formation (0.28±0.26 in comparison with 2.37±0.70 newly formed branchlets per 100 µm, *n*=5), whereas the rates of extension and partial or complete retraction were not affected (Fig. S2A,B,D; Movie 2). Hence, Arp2/3 complex promotes branching in cIVda neurons primarily by initiating *de novo* formation of dendrite branches.

To investigate the localization of the Arp2/3 complex during dendrite differentiation, we expressed GFP-tagged Arp3 (Arp3-GFP) in cIVda neurons of second instar larvae, under the control of *Gal4*^{ppk}, a condition that does not alter the morphology of cIVda neurons (data not shown). Arp3-GFP was enriched at discrete puncta (Fig. 2F; Movie 3). Newly forming branches were almost invariably marked by the presence of Arp3-GFP at the branching point (Fig. 2I, black line). Furthermore, Arp3-GFP localization marked the site of subsequent branch formation 60 s in advance (Fig. 2G-I). Thus, Arp3 localization strongly correlated with the formation of a new branchlet and predicted the site of branchlet formation. The localization was transient and the signal decreased rapidly again after the initiation of banchlet elongation (Fig. 2I). Consistently, we observed a decrease of Arp3-GFP fluorescence when branchlets disappeared (Fig. 2I). Taken together, the phenotypic characterization of Arp2/3 complex loss of function, together with the Arp3-GFP localization observed in live-cell imaging, suggest that the local recruitment of the Arp2/3 complex is an early step towards dendrite branch formation.

The nucleating activity of the Arp2/3 complex is intrinsically low and requires activation via interaction with the VCA (verprolin-homology, central, acidic) domain of Wilskott-Aldrich syndrome protein (WASP) family of proteins (Campellone and Welch, 2010). Using RNAi we knocked down the WASP family proteins characterized in fly in da neurons and found that only a reduction of the SCAR/ WAVE function resulted in a similar phenotype to the one observed upon loss of Arp2/3 function (Fig. S3). Cell type-specific knockdown of WAVE resulted in a reduction of branch number and density in cIIIda and cIVda neurons, and a reduction of branches in cIda (Fig. S3A-F). To validate the knockdown data, we generated single *wave*$^{\Delta 37}$ mutant cell clones by MARCM (Zallen et al., 2002). The densities of secondary, tertiary and higher-order branches in *wave*$^{\Delta 37}$ mutant class IV ddaC neurons were clearly reduced (Fig. 3B,C). Interestingly, a membrane-tagged WAVE construct lacking the VCA domain for Arp2/3 activation and acting

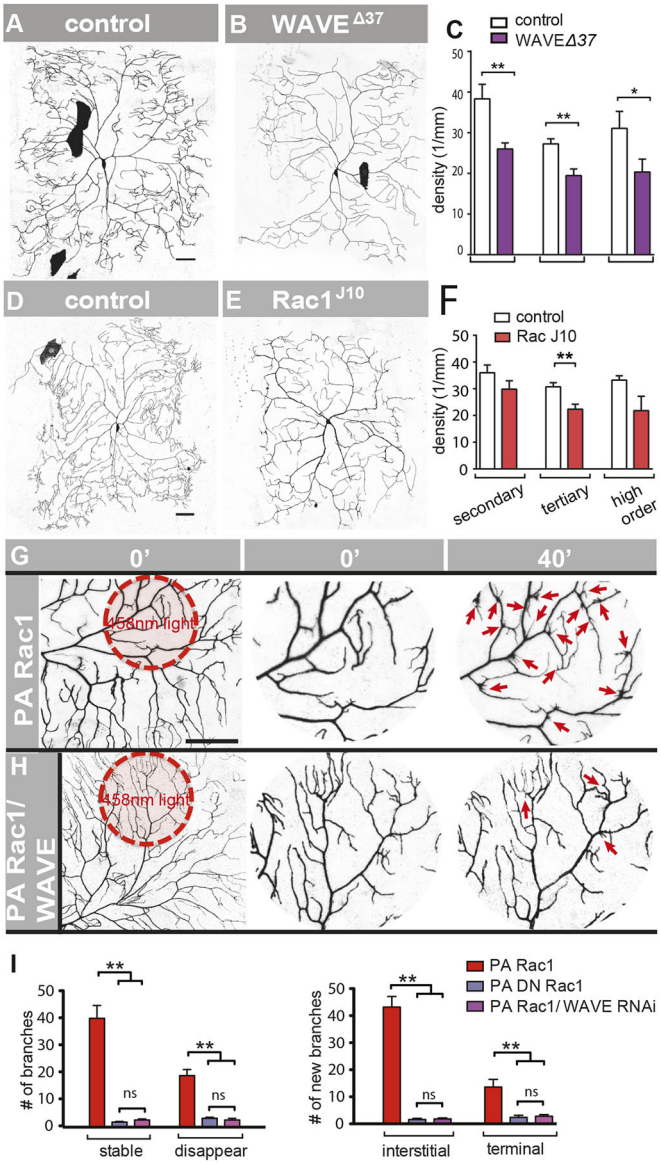

Fig. 3. WAVE and Rac1 control cIVda dendrite branch number. (A,B,D,E) Single ddaC cell clones obtained by MARCM of either control neurons (A,D) or neurons mutant for *wave* (*wave*$^{\Delta 37}$) (*n*=6) (B) or for *Rac1*^{J10} (*n*=4) (E). Scale bars: 50 µm. (C) The density of branches is reduced in *wave*$^{\Delta 37}$clones. (F) The density of tertiary dendrite branches is reduced in *Rac1*^{J10} mutant clones. (G,H) Images from time-lapse recordings of ddaC neurons expressing membrane-tagged red fluorescent *mCherry* and (G) photoactivatable constitutively active Rac1 (*PA Rac1*; Movie 4) or (H) *PA Rac1* and *Wave* RNAi-inducing constructs (*PA Rac1/ wave RNAi*; Movie 6) under the control of *ppk-Gal4*. The red circle represents the ROI illuminated with 458 nm light. Scale bar: 50 µm (left). *n*=5. The central and right panels show a magnification of the highlighted ROI circle prior to and after 40 min of photoactivation, respectively. The arrows indicate some of the newly formed single branchlets or groups of branchlets. (I) Quantification of the number of newly formed branches in the 40 min of imaging. *P≤0.05; **P≤0.01; ns, not significant (P>0.05).

as a dominant-negative (WAVE$^{\Delta VCAmyr}$) (Stephan et al., 2011) reproduced the *wave* mutant phenotype that displayed a reduction in the number and density of secondary, tertiary and higher-order branches (Fig. S4C,D). RNAi-mediated *wave* knockdown in ddaC neurons produced a strong reduction of *de novo* branch formation. The remaining dendritic branches appeared to be more stable and

Development (2019) 146, dev171397. doi:10.1242/dev.171397

less dynamic than the control (Fig. S2C,D; Movie 2). Thus, WAVE, like Arp2/3, is primarily required for *de novo* formation of dendrite branchlets. The activation and membrane recruitment of WAVE is in turn under tight regulation by the conserved multiprotein WAVE regulatory complex (WRC) (Chen et al., 2010). Within the WRC, the Sra-1 and Nap-1 dimer is essential for both Rac1-mediated regulation of the WRC and its recruitment to the membrane (Chen et al., 2010). *Sra-1* knockdown by RNAi yielded a similar effect to the loss of Arp2/3 or loss of WAVE, namely a clear reduction in the density of secondary and high-order branches of cIVda neurons (Fig. S4F,G). Together, these data suggest that WAVE is a major activator of Arp2/3 during dendrite branch formation in cIVda neurons.

The small GTPase Rac1 is a central determinant of cytoskeleton organization through the regulation of multiple proteins, including the WRC (Steffen et al., 2004; Tahirovic et al., 2010). Furthermore, da neurons overexpressing Rac1 display an increased number of terminal dendrite branchlets (Andersen et al., 2005; Emoto et al., 2004; Lee et al., 2003; Nagel et al., 2012). We therefore asked whether Rac1 drives the activation of WAVE and Arp2/3, and promotes dendrite branchlet formation. Single cIVda neuron MARCM clones mutant for Rac1 ($Rac1^{J10}$) (Hakeda-Suzuki et al., 2002) displayed a reduction in the number of tertiary branches (Fig. 3D-F), indicating that appropriate branching of cIVda neurons requires Rac1 (Lee et al., 2003; Nagel et al., 2012; Soba et al., 2015). Next, we used a photoactivatable form of a constitutively active mutated Rac1 protein (PA-Rac1CA) (Wang et al., 2010; Wu et al., 2009). When applying localized photoactivation in a restricted region of interest (ROI) of cIVda neurons, this construct was de-suppressed and produced strong and rapid formation of single branchlets and of groups of branchlets (Fig. 3G,I; Movie 4). Such an effect was not elicited in unilluminated ROIs upon overexpression of a dominant-negative PA-Rac1DN or of a light-insensitive LI PA-Rac1CA (Fig. S4H-J; Movie 5). A large fraction of the branchlets formed after illumination appeared along the length of existing dendrites, rather than at dendrite tips, and remained stable (Fig. 3I). Importantly, the dendrite overbranching locally induced by PA-Rac1CA was largely suppressed in the background of cell-autonomous *wave* RNAi (Fig. 3H,I; Movie 6). Thus, Rac1-induced branchlet formation requires WAVE in da neurons.

The Arp 2/3 complex binds to already existing actin filaments and is the only actin nucleator generating characteristic branched F-actin networks (Mullins et al., 1998). We thus attempted to locate the activity of the Arp2/3 complex in a structural context and carried out electron microscopy of dendrite branching points in primary neuronal cultures (Small et al., 2008). We obtained striking images of branching points of dendrites of larval brain neuron primary cultures (Fig. 4). In dendrite branches, we observed a few microtubules and long actin filaments extending parallel to the cortical membrane (Fig. 4B), similar to what has been reported for cultured rat hippocampal neurons (Xu et al., 2013). In contrast, the branchlets were filled by a tight bundle of actin filaments (Fig. 4F). However, we did not observe regions of branched actin filaments within the dendrite branchlets, as reported for the filopodia that give rise to dendrite spines (Korobova and Svitkina, 2010). At branching points, actin filaments appeared more dispersed and less bundled than along the main dendrites (Fig. 4B). Splayed microtubule filaments were present at branching points (Fig. 4B). In all analysed tomograms of branching points in dendrites (n=5 fully traced tomograms out of 12 sets), we observed several patches of short highly branched actin filaments (Fig. 4C-E,G). To follow the actin filaments in 3D and to unambiguously trace actin branching points, we performed EM tomography of dendrite branching points and reconstructed actin and microtubules (Fig. 4H; Movie 7). In the tilted images we could define unequivocally sites of actin branching (Movie 7), a clear indication of Arp2/3 activity. Single filaments derived from a patch of branched actin converged into actin bundles forming the core of a branchlet (Fig. 4F). Thus, patches of branched F-actin were specifically present at the base of dendritic branching points, supporting a role for Arp2/3 in dendrite branching.

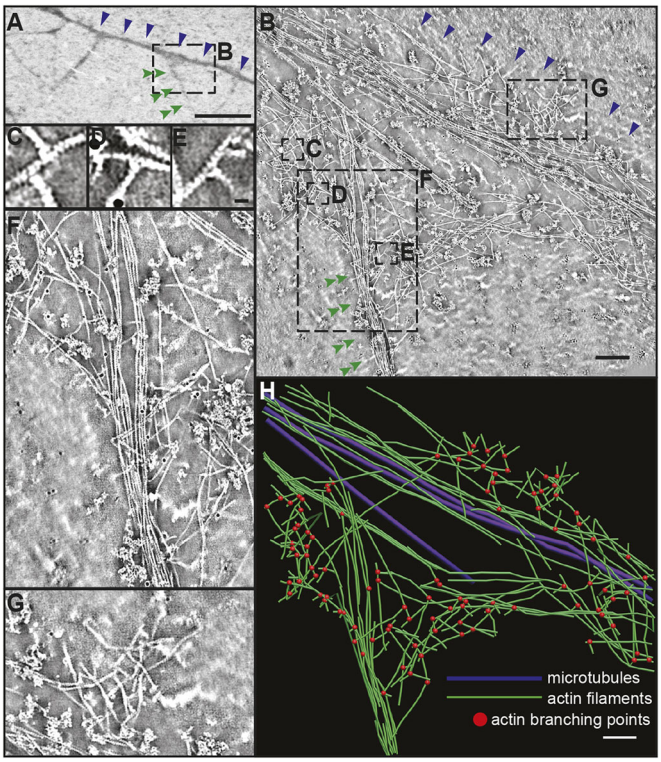

Fig. 4. Electron tomography reveals patches of branched actin at the base of dendrite branchlets. (A) Low-magnification image of a dendrite branch of a cultured larval brain neuron. Blue arrowheads indicate the dendrite branch. Green double arrowheads indicate a branchlet. Scale bar: 5 µm. (B) Electron tomogram image of the dendrite branching point boxed in A. Blue arrowheads indicate the dendrite branch shown in A. Green double arrowheads indicate the same branchlet as in A. Scale bar: 1 µm. The patches boxed in B are magnified in C-G. Scale bar in E: 100 nm. (F) Single filaments converge from the actin patches into the dendrite branchlet. (H) Still image from a 3D reconstruction of the tomogram shown in A. See also Movie 7. The red dots indicate the actin branching points. Scale bar: 1 µm.

The data presented here delineate a model of the mechanism underlying dendritic branching. This involves the initial activation of Rac1, leading to recruitment and local activation of the WRC. The subsequent transient recruitment of the Arp2/3 complex promotes the nucleation of branched actin filaments close to the plasma membrane that can thus be pushed forward to form an initial process.

One major trait of neuronal morphology is the density of dendrite branches (Stuart et al., 2007), which is likely produced by a combination of frequency of *de novo* branch formation and incidence of stabilization of the produced branchlets (Ziv and Smith, 1996). Our data indicate that the distribution of sites of Arp2/3 complex activation plays a major role in the control of branch formation frequency. Rac1 activity promotes actin recruitment at sites of dendrite spine formation and of dendrite filopodium initiation (Cheadle and Biederer, 2012; Galic et al., 2014; Korobova and Svitkina, 2010). Furthermore, Rac1 is responsible for the localization of WAVE at the growth cone

Development (2019) 146, dev171397. doi:10.1242/dev.171397

plasma membrane of mouse cerebellar granule neurons (Tahirovic et al., 2010). We thus hypothesize that activated Rac1 might recruit WRC at various locations along the length of a dendrite, but once a crucial concentration of active WAVE is reached, Arp2/3 can locally remodel the actin cytoskeleton to promote the formation of an actin patch. This cascade closely resembles the initiation of axonal branch formation (Armijo-Weingart and Gallo, 2017). In addition, the localization of WRC can be supported by a large family of molecules containing a short WRC interacting receptor sequence (WIRS) (Chen et al., 2014). In fact, molecular complexes including WIRS-containing proteins were recently shown to contribute to the localization of axon or dendrite branching sites in *C. elegans* HSN and PVD neurons, respectively, in part by binding to the WRC (Chia et al., 2014; Zou et al., 2018). The transmembrane receptor Robo, which promotes branching in cIVda neurons, contains a WIRS domain and might represent a potential candidate for the localization of WRC in these neurons to support branch formation (Chen et al., 2014; Dimitrova et al., 2008). How the localization of WIRS-containing activators might in turn become spatially restricted to initiate branch formation at discrete locations along the dendrite is not clear.

Taken together, we have revealed the details of the initial step into the formation of a dendrite branchlet *in vivo* with high temporal and spatial resolution. We suggest that, given the potential pathways of activation of WRC, in different neurons a concentration of active Arp2/3 that is sufficient for initiating branchlet formation might be achieved by stochastic enrichment of the activators or by the tethered localization of activator complexes at specific sites.

MATERIALS AND METHODS

Fly lines and genetics

All flies were kept at 25°C unless otherwise noted. The fly strains used are listed in the supplementary Materials and Methods. MARCM was performed as described by Nagel et al. (2012) (see supplementary Materials and Methods). For all RNAi experiments, animals carried a da neuron class-specific driver (*Gal4^{ppk}*, *Gal4^{IG11}* or *Gal4^{C161}*), *UAS-mCD8 GFP*, *UAS-Dcr2*, and a target or control RNAi. Embryos were allowed to develop at 25°C until examined as third instar larvae.

Microscopy

Live late third instar larvae expressing *UAS-mCD8GFP* in subsets of da neurons were mounted in 70% glycerol and immobilized with a cover slip for visualization with a Leica TCS SP2 confocal microscope. For time-lapse imaging, second instar live larvae expressing *UAS-mCD8GFP* in subsets of da neurons were immobilized in an imaging chamber (Dimitrova et al., 2008) filled with halocarbon oil to allow oxygen exchange, and confocal *z*-stacks (six images spaced by 1 µm) were obtained using a Carl Zeiss LSM7 confocal microscope every 5 min over a period of 30 min. Two-colour imaging of *Gal4$^{109(2)80}$/+; UAS-mCD8-Cherry/UAS-GMA* or *Gal4$^{109(2)80}$/+; UAS-mCD8-Cherry/UAS-Arp3-GFP* larvae was performed as previously described (Nagel et al., 2012) with several modifications. Briefly, for GMA, imaging stacks spaced by 1 µm were obtained every 30 s over a period of 10 min with a dual camera system; for Arp3 GFP, images were obtained every min over a period of 10-15 min with a single camera. In both cases, a Yokogawa Spinning-Disc on a Nikon stand (Andor) with two back-illuminated EM-CCD cameras (Andor iXON DU-897) was used. Two colour images of dual camera recordings were aligned automatically using Huygens essentials (Scientific Volume Imaging). Abdominal segment A6 was imaged for GMA and segments A1-2 for Arp3 GFP. Larvae expressing Arp3 GFP were kept at 29°C until imaging. To determine a point of new branch formation, newly forming branches were observed during the time-lapse images and their first appearance was set as the time-point 0 s. Accumulation of GMA was measured at the time point −30 s as the maximum intensity of a round region of interest (ROI) of 7 pixels diameter. A threshold for background GMA signal was set by averaging 20 randomly set ROIs along dendrite branches for each video (n=11). The spatiotemporal analysis of the Arp3-GFP signal along individual branches is described in detail in the supplementary Materials and Methods.

Photoactivation

All flies expressing photoactivatable constructs were raised under standard conditions but in full darkness. They carried: *ppk-Gal4 UAS-mCherry* and *UAS-PA Rac1 CA*, *UAS-PA DN Rac1*, *UAS-LI Rac1* or *UAS-PA Rac1 CA* and *UAS Wave* RNAi. Living late third instar larvae were prepared for live confocal imaging under a dimmed red light. Photoactivation of PA-Rac1 and live-cell imaging were performed using a Carl Zeiss LSM5 confocal microscope. To photoactivate the Rac1 constructs (CA, LI or DN), the indicated region of interest (ROI) of the dendritic tree of a ddaC neuron in living L3 larvae was repeatedly illuminated using a 5 mW 445 nm laser at 0.2% power for 20 s in a photobleaching mode and the membrane marker mCherry was imaged in the red channel every minute (Kato et al., 2014; Wu et al., 2009).

Image analysis and statistics

Quantification of a dendritic tree complexity was performed by manual tracing of dendritic branches from maximum projections of original image stacks in ImageJ using the NeuronJ plug-in and FIJI. Dendrites were separated in specific clusters (Figs S1, S3) according to their morphology and distance from the cell soma. Density was measured as number of branches of a given order divided by total length of lower order branches. Bar graphs and tables express the data of dendritic length and number as mean±s.e.m. Unless otherwise noted, data were analysed for statistical significance using two-tailed unpaired Student *t*-test for comparing two groups or one-way ANOVA for more than two groups at $P<0.05$. If normal distribution of the dataset was confirmed using the Shapiro-Wilk normality test, the ANOVA Bonferroni's post test was used for multiple comparison, otherwise the Krustal-Wallis test with a Dunn's post test was used. Asterisks in graphs and tables represent the significance of *P*-values comparing indicated groups with control (*$P<0.05$; **$P<0.01$; ***$P<0.001$; ****$P<0.0001$). For time-lapse analysis, every time point was analysed separately. At least five animals per genotype were used for quantification.

Electron microscopy and cell-culture

Electron microscopy experiments were obtained with primary neuronal culture of larval mushroom body neurons. Dissociated neuronal cultures from *Drosophila* brain tissue were prepared as described previously (Kraft et al., 2006) and cultured on formvar-coated gold finder EM grids for 48 h at 25°C. The cells were examined and preselected on an inverted Zeiss Observer epifluorescence microscope and extracted at room temperature with cytoskeleton buffer [10 mM MES buffer, 150 mM NaCl, 5 mM EGTA, 5 mM glucose, 5 mM $MgCl_2$ (pH 6.8)] containing 0.25% glutaraldehyde and 0.5% Triton for 40 s. For electron tomography, neurons were fixed with 2% glutaraldehyde in the same buffer for 15 min and grids were stained with 6-8% sodium silicotungstate (SST), including 1 mg/ml phalloidin. Electron tomography was obtained using an FEI Tecnai F30 Helium (Polara) microscope, and actin filaments were manually tracked using IMOD, as previously described (Mueller et al., 2014; Vinzenz et al., 2012).

Acknowledgements

We dedicate this manuscript to the family of our dear colleague Anastasia Tatarnikova, whom we prematurely lost during the course of this work. We are grateful to Dr Fikret-Gürkan Agircan for his great experimental support during revision. We thank J. Zallen for sharing fly lines and the Bloomington Stock Center for providing reagents. We are grateful to Rüdiger Klein (MPI of Neurobiology) for hosting A.T., to Michael Sixt (IST Austria) for his support, and to Frank Bradke and Peter Soba for helpful discussions and comments on the manuscript. Members of the Tavosanis lab provided many helpful comments.

Competing interests

The authors declare no competing or financial interests.

Author contributions

Conceptualization: T.S., A.T., H.C., G.T.; Methodology: T.S., A.T., J.M., B.S., H.C., M.N., V.S.; Software: B.S., H.C.; Formal analysis: T.S., A.T., J.M., B.S., H.C., G.T.;

Investigation: T.S., A.T., J.M., B.S., Y.Z., M.N.; Resources: H.C., S.B., V.S.; Writing - original draft: G.T.; Writing - review & editing: T.S., G.T.; Supervision: G.T.; Project administration: G.T.; Funding acquisition: G.T.

Funding
This work was supported by a Deutsche Forschungsgemeinschaft grant to G.T. (SPP 1464 TA 265/4), and by a Bundesministerium für Bildung und Forschung grant (01GQ1406-Bernstein Award 2013) and a Deutsche Forschungsgemeinschaft grant (CU 217/2-1) to H.C.

Supplementary information
Supplementary information available online at
http://dev.biologists.org/lookup/doi/10.1242/dev.171397.supplemental

References

Andersen, R., Li, Y., Resseguie, M. and Brenman, J. E. (2005). Calcium/calmodulin-dependent protein kinase II alters structural plasticity and cytoskeletal dynamics in Drosophila. *J. Neurosci.* **25**, 8878-8888. doi:10.1523/JNEUROSCI.2005-05.2005

Armijo-Weingart, L. and Gallo, G. (2017). It takes a village to raise a branch: cellular mechanisms of the initiation of axon collateral branches. *Mol. Cell. Neurosci.* **84**, 36-47. doi:10.1016/j.mcn.2017.03.007

Campellone, K. G. and Welch, M. D. (2010). A nucleator arms race: cellular control of actin assembly. *Nat. Rev. Mol. Cell Biol.* **11**, 237-251. doi:10.1038/nrm2867

Cheadle, L. and Biederer, T. (2012). The novel synaptogenic protein Farp1 links postsynaptic cytoskeletal dynamics and transsynaptic organization. *J. Cell Biol.* **199**, 985-1001. doi:10.1083/jcb.201205041

Chen, Z., Borek, D., Padrick, S. B., Gomez, T. S., Metlagel, Z., Ismail, A. M., Umetani, J., Billadeau, D. D., Otwinowski, Z. and Rosen, M. K. (2010). Structure and control of the actin regulatory WAVE complex. *Nature* **468**, 533-538. doi:10.1038/nature09623

Chen, B., Brinkmann, K., Chen, Z., Pak, C. W., Liao, Y., Shi, S., Henry, L., Grishin, N. V., Bogdan, S. and Rosen, M. K. (2014). The WAVE regulatory complex links diverse receptors to the actin cytoskeleton. *Cell* **156**, 195-207. doi:10.1016/j.cell.2013.11.048

Chia, P. H., Chen, B., Li, P., Rosen, M. K. and Shen, K. (2014). Local F-actin network links synapse formation and axon branching. *Cell* **156**, 208-220. doi:10.1016/j.cell.2013.12.009

Dailey, M. E. and Smith, S. J. (1996). The dynamics of dendritic structure in developing hippocampal slices. *J. Neurosci.* **16**, 2983-2994. doi:10.1523/JNEUROSCI.16-09-02983.1996

Dharmalingam, E., Haeckel, A., Pinyol, R., Schwintzer, L., Koch, D., Kessels, M. M. and Qualmann, B. (2009). F-BAR proteins of the syndapin family shape the plasma membrane and are crucial for neuromorphogenesis. *J. Neurosci.* **29**, 13315-13327. doi:10.1523/JNEUROSCI.3973-09.2009

D'Este, E., Kamin, D., Göttfert, F., El-Hady, A. and Hell, S. W. (2015). STED nanoscopy reveals the ubiquity of subcortical cytoskeleton periodicity in living neurons. *Cell Rep.* **10**, 1246-1251. doi:10.1016/j.celrep.2015.02.007

Dietzl, G., Chen, D., Schnorrer, F., Su, K.-C., Barinova, Y., Fellner, M., Gasser, B., Kinsey, K., Oppel, S., Scheiblauer, S. et al. (2007). A genome-wide transgenic RNAi library for conditional gene inactivation in Drosophila. *Nature* **448**, 151-156. doi:10.1038/nature05954

Dimitrova, S., Reissaus, A. and Tavosanis, G. (2008). Slit and Robo regulate dendrite branching and elongation of space-filling neurons in Drosophila. *Dev. Biol.* **324**, 18-30. doi:10.1016/j.ydbio.2008.08.028

Edwards, K. A., Demsky, M., Montague, R. A., Weymouth, N. and Kiehart, D. P. (1997). GFP-moesin illuminates actin cytoskeleton dynamics in living tissue and demonstrates cell shape changes during morphogenesis in Drosophila. *Dev. Biol.* **191**, 103-117. doi:10.1006/dbio.1997.8707

Emoto, K., He, Y., Ye, B., Grueber, W. B., Adler, P. N., Jan, L. Y. and Jan, Y.-N. (2004). Control of dendritic branching and tiling by the Tricornered-kinase/Furry signaling pathway in Drosophila sensory neurons. *Cell* **119**, 245-256. doi:10.1016/j.cell.2004.09.036

Firat-Karalar, E. N. and Welch, M. D. (2011). New mechanisms and functions of actin nucleation. *Curr. Opin. Cell Biol.* **23**, 4-13. doi:10.1016/j.ceb.2010.10.007

Galic, M., Tsai, F.-C., Collins, S. R., Matis, M., Bandara, S. and Meyer, T. (2014). Dynamic recruitment of the curvature-sensitive protein ArhGAP44 to nanoscale membrane deformations limits exploratory filopodia initiation in neurons. *Elife* **3**, e03116. doi:10.7554/eLife.03116

Gao, F.-B., Brenman, J. E., Jan, L. Y. and Jan, Y. N. (1999). Genes regulating dendritic outgrowth, branching, and routing in Drosophila. *Genes Dev.* **13**, 2549-2561. doi:10.1101/gad.13.19.2549

Govek, E.-E., Newey, S. E. and Van Aelst, L. (2005). The role of the Rho GTPases in neuronal development. *Genes Dev.* **19**, 1-49. doi:10.1101/gad.1256405

Grueber, W. B., Jan, L. Y. and Jan, Y. N. (2002). Tiling of the Drosophila epidermis by multidendritic sensory neurons. *Development* **129**, 2867-2878.

Hakeda-Suzuki, S., Ng, J., Tzu, J., Dietzl, G., Sun, Y., Harms, M., Nardine, T., Luo, L. and Dickson, B. J. (2002). Rac function and regulation during Drosophila development. *Nature* **416**, 438-442. doi:10.1038/416438a

Halachmi, N., Nachman, A. and Salzberg, A. (2012). Visualization of proprioceptors in Drosophila larvae and pupae. *J. Vis. Exp.* **64**, e3846. doi:10.3791/3846

Heiman, M. G. and Shaham, S. (2010). Twigs into branches: how a filopodium becomes a dendrite. *Curr. Opin. Neurobiol.* **20**, 86-91. doi:10.1016/j.conb.2009.10.016

Hudson, A. M. and Cooley, L. (2002). A subset of dynamic actin rearrangements in Drosophila requires the Arp2/3 complex. *J. Cell Biol.* **156**, 677-687. doi:10.1083/jcb.200109065

Jan, Y.-N. and Jan, L. Y. (2010). Branching out: mechanisms of dendritic arborization. *Nat. Rev. Neurosci.* **11**, 316-328. doi:10.1038/nrn2836

Jontes, J. D., Buchanan, J. and Smith, S. J. (2000). Growth cone and dendrite dynamics in zebrafish embryos: early events in synaptogenesis imaged in vivo. *Nat. Neurosci.* **3**, 231-237. doi:10.1038/72936

Kaethner, R. J. and Stuermer, C. A. (1997). Dynamics of process formation during differentiation of tectal neurons in embryonic zebrafish. *J. Neurobiol.* **32**, 627-639. doi:10.1002/(SICI)1097-4695(19970605)32:6<627::AID-NEU7>3.0.CO;2-1

Kato, T., Kawai, K., Egami, Y., Kakehi, Y. and Araki, N. (2014). Rac1-dependent lamellipodial motility in prostate cancer PC-3 cells revealed by optogenetic control of Rac1 activity. *PLoS ONE* **9**, e97749. doi:10.1371/journal.pone.0097749

Korobova, F. and Svitkina, T. (2010). Molecular architecture of synaptic actin cytoskeleton in hippocampal neurons reveals a mechanism of dendritic spine morphogenesis. *Mol. Biol. Cell* **21**, 165-176. doi:10.1091/mbc.e09-07-0596

Kraft, R., Escobar, M. M., Narro, M. L., Kurtis, J. L., Efrat, A., Barnard, K. and Restifo, L. L. (2006). Phenotypes of Drosophila brain neurons in primary culture reveal a role for fascin in neurite shape and trajectory. *J. Neurosci.* **26**, 8734-8747. doi:10.1523/JNEUROSCI.2106-06.2006

Lee, T. and Luo, L. (1999). Mosaic analysis with a repressible cell marker for studies of gene function in neuronal morphogenesis. *Neuron* **22**, 451-461. doi:10.1016/S0896-6273(00)80701-1

Lee, A., Li, W., Xu, K., Bogert, B. A., Su, K. and Gao, F. B. (2003). Control of dendritic development by the Drosophila fragile X-related gene involves the small GTPase Rac1. *Development* **130**, 5543-5552. doi:10.1242/dev.00792

Mueller, J., Pfanzelter, J., Winkler, C., Narita, A., Le Clainche, C., Nemethova, M., Carlier, M.-F., Maeda, Y., Welch, M. D., Ohkawa, T. et al. (2014). Electron tomography and simulation of baculovirus actin comet tails support a tethered filament model of pathogen propulsion. *PLoS Biol.* **12**, e1001765. doi:10.1371/journal.pbio.1001765

Mullins, R. D., Heuser, J. A. and Pollard, T. D. (1998). The interaction of Arp2/3 complex with actin: nucleation, high affinity pointed end capping, and formation of branching networks of filaments. *Proc. Natl. Acad. Sci. USA* **95**, 6181-6186. doi:10.1073/pnas.95.11.6181

Nagel, J., Delandre, C., Zhang, Y., Forstner, F., Moore, A. W. and Tavosanis, G. (2012). Fascin controls neuronal class-specific dendrite arbor morphology. *Development* **139**, 2999-3009. doi:10.1242/dev.077800

Niell, C. M., Meyer, M. P. and Smith, S. J. (2004). In vivo imaging of synapse formation on a growing dendritic arbor. *Nat. Neurosci.* **7**, 254-260. doi:10.1038/nn1191

Nithianandam, V. and Chien, C.-T. (2018). Actin blobs prefigure dendrite branching sites. *J. Cell Biol.* **217**, 3731-3746. doi:10.1083/jcb.201711136

Rottner, K., Faix, J., Bogdan, S., Linder, S. and Kerkhoff, E. (2017). Actin assembly mechanisms at a glance. *J. Cell Sci.* **130**, 3427-3435. doi:10.1242/jcs.206433

Saarikangas, J., Kourdougli, N., Senju, Y., Chazal, G., Segerstrale, M., Minkeviciene, R., Kuurne, J., Mattila, P. K., Garrett, L., Hölter, S. M. et al. (2015). MIM-induced membrane bending promotes dendritic spine initiation. *Dev. Cell* **33**, 644-659. doi:10.1016/j.devcel.2015.04.014

Singhania, A. and Grueber, W. B. (2014). Development of the embryonic and larval peripheral nervous system of Drosophila. *Wiley Interdiscip Rev. Dev. Biol.* **3**, 193-210. doi:10.1002/wdev.135

Small, J. V., Auinger, S., Nemethova, M., Koestler, S., Goldie, K. N., Hoenger, A. and Resch, G. P. (2008). Unravelling the structure of the lamellipodium. *J. Microsc.* **231**, 479-485. doi:10.1111/j.1365-2818.2008.02060.x

Soba, P., Han, C., Zheng, Y., Perea, D., Miguel-Aliaga, I., Jan, L. Y. and Jan, Y. N. (2015). The Ret receptor regulates sensory neuron dendrite growth and integrin mediated adhesion. *Elife* **4**, e05491. doi:10.7554/eLife.05491

Steffen, A., Rottner, K., Ehinger, J., Innocenti, M., Scita, G., Wehland, J. and Stradal, T. E. B. (2004). Sra-1 and Nap1 link Rac to actin assembly driving lamellipodia formation. *EMBO J.* **23**, 749-759. doi:10.1038/sj.emboj.7600084

Stephan, R., Gohl, C., Fleige, A., Klämbt, C. and Bogdan, S. (2011). Membrane-targeted WAVE mediates photoreceptor axon targeting in the absence of the WAVE complex in Drosophila. *Mol. Biol. Cell* **22**, 4079-4092. doi:10.1091/mbc.e11-02-0121

Stuart, G., Spruston, N. and Häusser, M. (2007). *Dendrites*, 2nd edn. Oxford; New York: Oxford University Press.

Sugimura, K., Yamamoto, M., Niwa, R., Satoh, D., Goto, S., Taniguchi, M., Hayashi, S. and Uemura, T. (2003). Distinct developmental modes and lesion-

induced reactions of dendrites of two classes of Drosophila sensory neurons. *J. Neurosci.* **23**, 3752-3760. doi:10.1523/JNEUROSCI.23-09-03752.2003

Tahirovic, S., Hellal, F., Neukirchen, D., Hindges, R., Garvalov, B. K., Flynn, K. C., Stradal, T. E., Chrostek-Grashoff, A., Brakebusch, C. and Bradke, F. (2010). Rac1 regulates neuronal polarization through the WAVE complex. *J. Neurosci.* **30**, 6930-6943. doi:10.1523/JNEUROSCI.5395-09.2010

Vinzenz, M., Nemethova, M., Schur, F., Mueller, J., Narita, A., Urban, E., Winkler, C., Schmeiser, C., Koestler, S. A., Rottner, K. et al. (2012). Actin branching in the initiation and maintenance of lamellipodia. *J. Cell Sci.* **125**, 2775-2785. doi:10.1242/jcs.107623

Wang, X., He, L., Wu, Y. I., Hahn, K. M. and Montell, D. J. (2010). Light-mediated activation reveals a key role for Rac in collective guidance of cell movement in vivo. *Nat. Cell Biol.* **12**, 591-597. doi:10.1038/ncb2061

Willig, K. I., Steffens, H., Gregor, C., Herholt, A., Rossner, M. J. and Hell, S. W. (2014). Nanoscopy of filamentous actin in cortical dendrites of a living mouse. *Biophys. J.* **106**, L01-L03. doi:10.1016/j.bpj.2013.11.1119

Wu, G. Y., Zou, D. J., Rajan, I. and Cline, H. (1999). Dendritic dynamics in vivo change during neuronal maturation. *J. Neurosci.* **19**, 4472-4483. doi:10.1523/JNEUROSCI.19-11-04472.1999

Wu, Y. I., Frey, D., Lungu, O. I., Jaehrig, A., Schlichting, I., Kuhlman, B. and Hahn, K. M. (2009). A genetically encoded photoactivatable Rac controls the motility of living cells. *Nature* **461**, 104-108. doi:10.1038/nature08241

Xu, K., Zhong, G. and Zhuang, X. (2013). Actin, spectrin, and associated proteins form a periodic cytoskeletal structure in axons. *Science* **339**, 452-456. doi:10.1126/science.1232251

Zallen, J. A., Cohen, Y., Hudson, A. M., Cooley, L., Wieschaus, E. and Schejter, E. D. (2002). SCAR is a primary regulator of Arp2/3-dependent morphological events in Drosophila. *J. Cell Biol.* **156**, 689-701. doi:10.1083/jcb.200109057

Zhang, S.-X., Duan, L.-H., He, S.-J., Zhuang, G.-F. and Yu, X. (2017). Phosphatidylinositol 3,4-bisphosphate regulates neurite initiation and dendrite morphogenesis via actin aggregation. *Cell Res.* **27**, 253-273. doi:10.1038/cr.2017.13

Ziv, N. E. and Smith, S. J. (1996). Evidence for a role of dendritic filopodia in synaptogenesis and spine formation. *Neuron* **17**, 91-102. doi:10.1016/S0896-6273(00)80283-4

Zou, W., Dong, X., Broederdorf, T. R., Shen, A., Kramer, D. A., Shi, R., Liang, X., Miller, D. M., III, Xiang, Y. K., Yasuda, R. et al. (2018). A Dendritic guidance receptor complex brings together distinct actin regulators to drive efficient F-actin assembly and branching. *Dev. Cell* **45**, 362-375.e363. 10.1016/j.devcel.2018.04.008